Quest to enhance up-conversion efficiency: a comparison of anhydrous vs. hydrous synthesis of NaGdF4: Yb3+ and Tm3+ nanoparticles

Bhagyesh Purohit, David Amans, Yannick Guyot, Benoit Mahler, Marie-France Joubert, Christophe Dujardin, S. Daniele, G. Ledoux, S. Mishra

Quest to enhance up-conversion efficiency: A comparison of anhydrous *versus* hydrous synthesis of $NaGdF_4$: Yb^{+3}, Tm^{+3} nanoparticles

Bhagyesh Purohit,[a,b] David Amans,[b] Yannick Guyot,[b] Benoit Mahler,[b] Marie-France Joubert,[b] Christophe Dujardin,[b] Stephane Daniele,[c] Gilles Ledoux,[b] and Shashank Mishra[a*]

[a] Univ Lyon, Université Claude Bernard Lyon 1, CNRS, Institut de Recherches sur l'Environnement et la Catalyse de Lyon, 69626, Villeurbanne, France.

[b] Univ Lyon, Université Claude Bernard Lyon 1, CNRS, Institut Lumière Matière, 69622, Villeurbanne, France.

[c] Univ Lyon, Université Claude Bernard Lyon 1, CNRS, ESCPE-Lyon, C2P2, BP 2077, 69616 Villeurbanne, France.

E-mail: shashank.mishra@ircelyon.univ-lyon1.fr

Abstract:

A major challenge in the field of up-converting (UC) nanomaterials is to enhance their efficiencies. The –OH defects on the surface of the nanoparticles are thought to be the main cause of luminescence quenching, but there are no comparative studies in the literature showing the impact of anhydrous *versus* hydrous synthesis on up-conversion efficiency. In this article, we present the synthesis of up-converting $NaGdF_4$: Yb^{+3}, Tm^{+3} nanoparticles by two different methods: Thermal decomposition of single source metal-organic anhydrous precursors [$NaLn(TFA)_4$(diglyme)] (Ln

= Gd, Tm, Yb; TFA = trifluoroacetate) and room temperature co-precipitation using hydrated inorganic salts $Ln(NO_3)_3 \cdot 5H_2O$ (Ln = Gd, Tm, Yb), $NaNO_3$ and NH_4F in ethylene glycol. After a detailed study on the influence of solvents and the percentage of lanthanide dopant on the crystal phase of the up-converting nanoparticles (NPs) and their complete characterization, a comparative up-conversion study was carried out which revealed that the uniform nanospheres (av. size ~13 nm) obtained from the anhydrous SSP had significantly higher up-conversion efficiency than agglomerated nanorods (~197 nm in length and ~95 nm in width) produced from hydrated inorganic salts. An enhanced up-conversion quantum yield of 1.8% for the anhydrous sample validates the anhydrous precursor approach as a strategy to obtain small but highly emitting up-converting particles without requiring a silica or undoped matrix surface passivation layer.

Key words: single source precursor; $NaGdF_4$, nanoparticles; anhydrous synthesis; up-conversion; quantum yield.

1. Introduction

Lanthanide-doped up-converting (Ln-UC) nanomaterials, which convert infrared radiation into UV-visible luminescence, continue to attract huge attention because of their potential applications in various fields ranging from biological imaging and therapeutics to photovoltaics, photonics and photocatalysis, as summarized in several recent review articles [1-14]. However, compared to conventional phosphors, the quantum yields of these Ln-UC nanoparticles are extremely low (typically <1%) and, in general, an order of magnitude lower than those of the corresponding up-conversion bulk materials [15]. Therefore, a major challenge for these materials is to enhance up-conversion luminescence. General criteria for achieving this goal include i) selection of a suitable

host matrix with low phonon energy (e.g., metal fluoride), ii) selection of an efficient crystal phase, and iii) optimization of the concentration of doping lanthanide ions [16].

A carefully chosen synthetic strategy for these UC nanomaterials allows the above criteria to be fulfilled by providing control over particle size, shape, dispersion and surface properties, which influence all up-conversion emission properties [17]. Bottom-up synthesis of nanomaterials using a precursor that contains all the constituent elements in the required ratio (single source precursor), facilitates better control over the composition, structure and morphology of nanomaterials [18, 19]. It is well-known that –OH defects in nanoparticles are the primary cause of luminescence quenching [20]. It is generally accepted that the construction of a shell of silica or undoped matrix (e.g., $NaYF_4$, $NaGdF_4$, etc.) around the up-converting core is an effective way to improve the UC luminescence of the UC NPs by confining Ln^{3+} dopant ions to the inner core, thus reducing non-radiative transitions [21,22]. However, this strategy cannot be used universally for all types of applications, especially for those requiring construction of additional layers of another material or necessitating short distances in view of specific interactions with grafted species, e.g., in photocatalysis [5]. Since our interest in Ln-UC materials is motivated by the potential application of TiO_2@UC NPs type core-shell structure for IR-induced photocatalysis [24], we have focused on the synthesis of smaller UC particles with strong emission without having a silica surface passivation layer or an undoped matrix. We have previously used anhydrous molecular precursors as a synthetic strategy to minimize –OH functionality at the surface of Ln-UC NPs [23-25], although no effort has been made to compare their up-conversion efficiency with UC materials produced through hydrous synthesis. Literature on the anhydrous synthesis of UC nanomaterials and its influence on up-conversion intensity is scarce [26]. In this article, we report the synthesis of up-converting (UC) $NaGdF_4$: Yb^{+3}, Tm^{+3} NPs by two different methods: thermal decomposition

of anhydrous metal-organic single source precursors [NaLn(TFA)$_4$(diglyme)] (Ln = Gd, Tm, Yb) and room temperature co-precipitation using hydrated inorganic salts Ln(NO$_3$)$_3$·5H$_2$O, NaNO$_3$ and NH$_4$F in ethylene glycol. After a detailed study of the influence of the solvents and the dopant percentage on the crystalline phase of the NPs obtained and their complete characterization, the UC NPs synthesized by these two strategies were studied for their up-conversion efficiency. These results reveal that uniform nanospheres with an average size of 13 nm obtained from anhydrous SSPs had a higher up-conversion intensity than agglomerated nanorods (~197 in length and ~95 nm in width) produced from hydrated inorganic salts.

2. Materials and methods

2.1. General Procedures. While all manipulations related to the anhydrous synthesis were carried out in an argon atmosphere using Schlenk tube and vacuum line techniques, the hydrous syntheses were performed in air. The solvents, trifluoroacetic acid (TFAH), diglyme, 1-octadecene (ODE), oleic acid (OA) and oleylamine (OM) (all Aldrich) were used as received. The purification of the solvents used in the synthesis of the anhydrous precursors (THF, diethylether and hexane) was achieved on a MB SPS-800 instrument. FT-IR spectra were recorded as KBr pellets on a Bruker Vector 22 spectrometer. The single source precursors [NaLn(TFA)$_4$(diglyme)] (Ln = Gd, Tm, Yb; TFA = trifluoroacetate), were prepared as described in our previous publications [23,24]. Powder X-ray diffraction data were obtained with a Siemens D 5000 diffractometer using CuKα radiation. Thermogravimetric (TGA) data for the as-prepared Ln^{3+}-doped NaGdF$_4$ nanoparticles were recorded in air on a Setaram 92 system in the temperature range 20–600 °C with a temperature ramp of 5 °Cmin^{-1}. Transmission electron microscopy (TEM) was performed on a JEOL JEM-2100

LaB_6 microscope operated at 200 kV. Using a homemade spectrofluorometer, up-conversion studies were carried out on dried and properly ground powders, which were placed on a sample holder with utmost care to ensure a flat and uniform deposition. The samples were irradiated with a continuous wave (CW) laser at 972 nm which was focused to a square spot of 1 × 1 mm^2 on the sample with a quasi-top-hat energy distribution. All the measurements were performed at an excitation power density of 16.5 W/cm^2. The emitted signal was then collected using Jobin-Yvon (TRIAX 320) monochromater equipped with automatic order removing filters and coupled to a cooled photomultiplier (Hamamatsu R943-02). The signal from the photomultiplier was sent to an SR400 counting module from Stanford Research Systems.

To measure the up-conversion quantum yield, the chosen Ln^{3+}-doped $NaGdF_4$ samples (6-12 months old) were placed in an integrating sphere (IS200-4 from Thorlabs) and excited from above with one end of the sphere connected to the detection system. To ensure that the detection system obtains the absolute response at each wavelength, it was calibrated using an Oriel QT 63358 tungsten lamp traceable by NIST over the range 250-1000 nm. In order to determine the absorption of 972 nm photons by the above samples, an undoped $NaGdF_4$ was prepared under identical conditions. The difference in laser scattering compared to doped and undoped samples gave us an estimate of the actual absorption of the laser by the sample. Thus, the actual number of absorbed photons (respective energy absorbed) and the actual number of emitted photons (respective energy emitted) were measured over the wavelength range from 250 nm to 1000 nm. The quantum up-conversion efficiency (energy conversion efficiency) is the ratio of emitted photons (emitted power) to absorbed photons (absorbed power).

2.2. Anhydrous synthesis of undoped $NaGdF_4$ and doped $NaGdF_4$: Yb^{+3}, Tm^{+3} nanoparticles from the thermal decomposition of the designed precursors [$NaLn(TFA)_4$(diglyme)] (Ln = Gd, Tm, Yb). A typical method of obtaining $NaGdF_4$ nanoparticles involved taking the precursor [$NaGd(TFA)_4$(diglyme)] in 4 ml of 1-octadecene (or a mixture of 2 ml each of ODE + OM or ODE + OA) to obtain solution A, which was then kept at 120 °C for 1h to obtain a ~~h~~ clear and homogeneous solution. In parallel, 6 ml of 1-octadecene (or a mixture of 3 ml each of ODE + OM or ODE + OA) was purged with argon and heated to 290 °C (solution B). When the temperature became constant at 290 °C for solution B, the pre-heated solution A (at 120 °C) was injected all at once. The reaction mixture was then stirred at 290 °C for 1h. It was then gradually cooled down to room temperature under a constant flow of argon. To collect the nanocrystals, ethanol was added as a precipitating agent, followed by centrifugation at 4500 rpm for 5 min. The resulting powder was washed three times with ethanol to remove any organic impurities and then air-dried at room temperature for 24h.

To prepare $NaGdF_4$: Yb^{+3}, Tm^{+3} nanoparticles, the isostructral precursors [$NaGd(TFA)_4$(diglyme)], [$NaYb(TFA)_4$(diglyme)] and [$NaTm(TFA)_4$(diglyme)] were taken in appropriate amounts and simultaneously decomposed as described above. Details concerning the amount of reactants, solvents, etc. are summarized in Table S1 in the supporting information.

2.3. Hydrous synthesis of $NaGdF_4$: Yb^{+3}, Tm^{+3} NPs from co-precipitation reaction of hydrated inorganic salts at room temperature. A typical method involves preparation of two different ethylene glycol solutions. Solution A consists of appropriate amounts of $Gd(NO_3)_3$, $Yb(NO_3)_3$, $Tm(NO_3)_3$ and $NaNO_3$ in 10 ml of ehtylene glycol, and solution B consists of an

appropriate amount of NH_4F in 20 ml of ethylene glycol. Solution A, containing all the nitrate precursors, was then added dropwise to solution B with vigorous stirring. This mixture was then stirred for 3h at room temperature, producing a transparent colloidal suspension. Finally, the $NaGdF_4$: *x*%Yb^{3+}, *y*%Tm^{3+} nanoparticles were collected by centrifugation (5000 rpm, 10 min), and further washed three times with ethanol and deionized water to remove any impurities. The resulting powder was then dried overnight at room temperature. The synthetic details of $NaGdF_4$ NPs doped with different amount of Yb^{3+} and Tm^{3+} ions are summarized in Table S2 in the supporting information.

3. Results and discussion

3.1. Anhydrous synthesis of $NaGdF_4$: Yb^{+3}, Tm^{+3} nanoparticles from thermal decomposition of designed precursors [$NaLn(TFA)_4$(diglyme)] (Ln = Gd, Tm, Yb): Influence of solvents and dopant percentage on the crystal phase of up-converting NPs.

The decomposition of the precursor [$NaGd(TFA)_4$(diglyme)] in a non-coordinating solvent 1-octadecene (ODE) at 290 °C, which afforded the β-phase of the $NaGdF_4$ NPs (ICDD # 00-027-0699), has been described by our group [24]. Although this precursor provides *in situ* the coordinating diglyme ligand, which acts as a surfactant for the $NaGdF_4$ NPs, it is less effective than widely used capping ligands such as oleic acid (OA) and oleylamine (OM) in controlling the nanoparticle size and dispersing them in the organic medium. We have, therefore, carried out here a systematic study on the thermal decomposition of this precursor in the mixed reaction medium containing different ratios of ODE, OM and OA. As observed for 1-octadecene, the decomposition of the Na-Gd heterometallic precursor in a 1:1 mixture of ODE + OA resulted in the β-phase of $NaGdF_4$ (bottom curve in the Fig. 1a), although a small percentage of GdF_3 NPs was also present,

probably due to the partial destruction of the Na-Gd heterometallic into homometallic components due to the possible replacement of the diglyme/TFA groups with oleate ligands. *In situ* substitution of the acetate group by the oleate ligand has previously been observed [19]. However, the presence of GdF_3 could be suppressed if the decomposition was carried out in the presence of NaTFA (up to 0.25 equivalent). On the other hand, the bottom curve in the Fig. 1b shows that the Na-Gd precursor decomposed in a 1:1 mixture of ODE + OM to give the pure α-phase of the $NaGdF_4$ NPs (ICDD # 00-027-0698). This result contrasts with the previous observation where the addition of OM promoted the formation of the β-phase over the α-phase for $NaYbF_4$ UC NPs [27].

Another critical criterion of UC efficiency is the doping ratio of co-doped lanthanide ions (sensitizer and activator), which needs to be optimized to maximize energy transfer but, at the same time, to minimize the loss of cross-relaxation energy [28]. To obtain the host matrix $NaGdF_4$ NPs co-doped with different percentages of Yb^{3+} and Tm^{3+} cations, the precursors $[NaLn(TFA)_4(diglyme)]$ (Ln = Gd, Tm, Yb) were taken in appropriate amounts and then simultaneously decomposed in a suitable mixture of solvents. These sets of up-converting nanoparticles obtained under strict anhydrous conditions are collectively abbreviated as UC_anhyd NPs. In general, while the increase in the percentage of Yb favors the formation of the α-phase, no clear trend was obtained in the case of thullium. Thus, the mixed α- and β-phases obtained for $NaGd_{5/6}Yb_{1/6}F_4$: 1% Tm^{3+} in the reaction medium ODE + OA are converted into pure α-phase when increasing the amount of Yb to 25% and more (Fig. 1a). We have already reported that the tendency to get the α-phase increases for late lanthanides with smaller radii [23, 24]. On the other hand, for a low percentage of Yb (17%), increasing the content of Tm^{3+} ions increases the percentage of the β-phase of the matrix. Thus, while a pure α- phase is obtained for $NaGd_{5/6}Yb_{1/6}F_4$: 0.4% Tm^{3+} in ODE + OM reaction medium, increasing the content of Tm to 0.8% introduces about 27% of the

β-phase, which further increases to 37% by raising the amount of Tm to 1.2%. However, no such influence of Tm^{3+} ions was present on doubling the amount of ytterbium in the matrix, as exemplified by $NaGd_{2/3}Yb_{1/3}F_4$: 0.3% Tm^{3+} and $NaGd_{2/3}Yb_{1/3}F_4$: 0.6% Tm^{3+} NPs which display about same amount of the β-phase (~9%). In summary, the use of single source precursors under different reaction media provides a robust and reproducible strategy for synthesizing a set of Ln^{3+}-doped $NaGdF_4$ UC NPs in pure α- or mixed α + β phases with defined ratios, the later can be converted easily to pure β-phase by calcination at 350 °C, with a slight agglomeration but without any significant change in the particle size (Fig. S1). Getting Ln^{3+}-doped $NaGdF_4$ UC NPs in pure α-, pure β- or mixed α + β phases is important given the different potential applications of the different polymorphs [29]. Table 1 summarizes the relative ratio of α- and/or β- crystalline phases, calculated after Rietveld refinement, and the crystallite size of the $NaGdF_4$: Yb^{+3}, Tm^{+3}_anhyd NPs obtained in different reaction media.

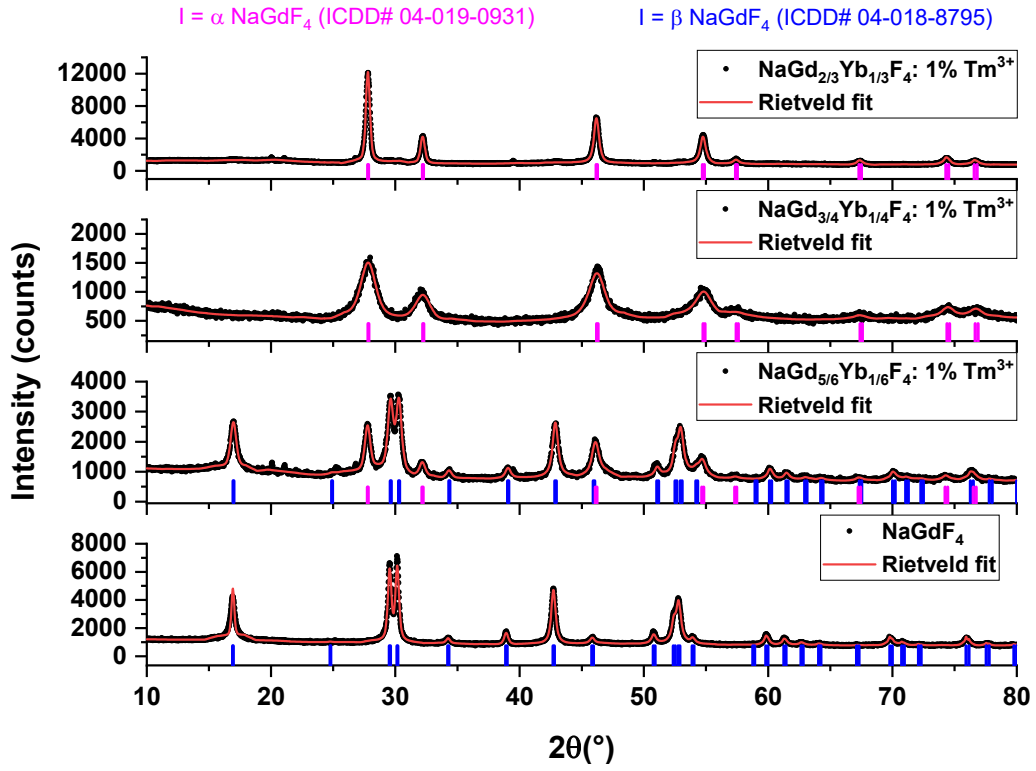
I = α NaGdF4 (ICDD# 04-019-0931)
I = β NaGdF4 (ICDD# 04-018-8795)
NaGd2/3Yb1/3F4: 1% Tm3+
Rietveld fit
NaGd3/4Yb1/4F4: 1% Tm3+
Rietveld fit
NaGd5/6Yb1/6F4: 1% Tm3+
Rietveld fit
NaGdF4
Rietveld fit
Intensity (counts)
2θ(°)

a)

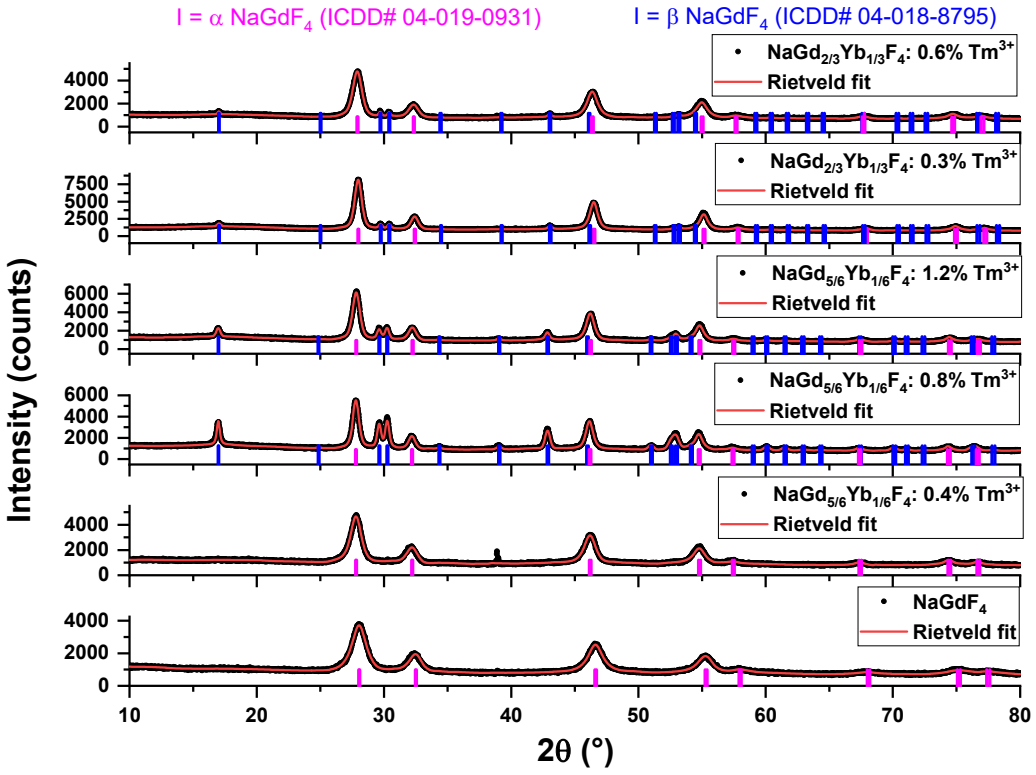
I = α NaGdF4 (ICDD# 04-019-0931)
I = β NaGdF4 (ICDD# 04-018-8795)
NaGd2/3Yb1/3F4: 0.6% Tm3+
Rietveld fit
NaGd2/3Yb1/3F4: 0.3% Tm3+
Rietveld fit
NaGd5/6Yb1/6F4: 1.2% Tm3+
Rietveld fit
NaGd5/6Yb1/6F4: 0.8% Tm3+
Rietveld fit
NaGd5/6Yb1/6F4: 0.4% Tm3+
Rietveld fit
NaGdF4
Rietveld fit
Intensity (counts)
2θ (°)

b)

Figure 1. Powder XRD of $NaGdF_4$: Yb^{3+}, Tm^{3+} NPs obtained from the thermal decomposition of SSPs in 1:1 mixture of ODE + OA (a) or ODE + OM (b).

Table 1. Different crystalline phases and crystallite size of the $NaGdF_4$: Yb^{+3}, Tm^{+3} NPs obtained from the thermal decomposition of SSPs [$NaLn(TFA)_4$(diglyme)] (Ln = Gd, Yb, Tm) at 290 °C in 1:1 mixture of 1-octadecene + oleic acid or 1-octadecene + oleylamine.

Molecular precursor	**Composition, crystalline phase and crystallite size (from Scherrer equation) of UC NPs**	
	ODE + OA	ODE + OM
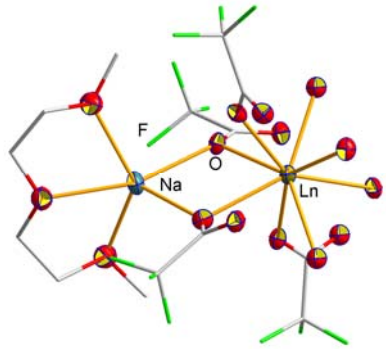 [$NaLn(TFA)_4$(diglyme)] (Ln = Gd, Tm, Yb; TFA = trifluoroacetate)	$NaGdF_4$ β (~19 nm)	$NaGdF_4$ α (~7 nm)
	-	$NaGd_{5/6}Yb_{1/6}F_4$: 0.4% Tm^{3+} α (~16 nm)
	$NaGd_{5/6}Yb_{1/6}F_4$: 1% Tm^{3+} α (13%) + β (87%) (~13 nm)	$NaGd_{5/6}Yb_{1/6}F_4$: 0.8% Tm^{3+} α (73%) + β (27%) (~18 nm)
	-	$NaGd_{5/6}Yb_{1/6}F_4$: 1.2% Tm^{3+} α (63%) + β (37%) (~16 nm)
	$NaGd_{3/4}Yb_{1/4}F_4$: 1% Tm^{3+} α (~6 nm)	-
	-	$NaGd_{2/3}Yb_{1/3}F_4$: 0.3% Tm^{3+} α (91%) + β (9%) (~19 nm)
	$NaGd_{2/3}Yb_{1/3}F_4$: 1% Tm^{3+} α (~18 nm)	$NaGd_{2/3}Yb_{1/3}F_4$: 0.6% Tm^{3+} α (92%) + β (8%) (~9 nm)

TEM images of these nanoparticles produced by the thermal decomposition method show that they are almost spherical and less than 20 nm in size (Fig. 2, S2, S3). Figure 2 corresponds to the TEM, HR-TEM and associated FFT of the sample $NaGd_{5/6}Yb_{1/6}F_4$: 0.8% Tm^{3+} containing the two

phases α and β. These images exhibit nearly spherical morphology and a controlled size distribution (13.7 ± 3.5 nm) for these nanoparticles (Fig. S4). The observed morphology is comparable to that of $NaGdF_4$ reported by the microwave-assisted decomposition of $[Ln(TFA)_3]$, although the particle size in this study was smaller due to a short reaction time (10 min in the microwave-assisted decomposition *vs* 1 h in the thermal decomposition) [19]. The presence of a mixture of phases (α + β), as shown by the XRD, was confirmed by HR-TEM analysis. The HR-TEM image in the Fig. 2b shows two particles with α- and β-phase, respectively. While the central particle with an interreticular spacing of 0.302 nm is related to the β-phase (Fig. 2c), the FFT of the second particle displayed in Fig. 2d shows the diffraction pattern of a cubic crystal structure (α-phase) in the zone axis [01-1] displayed in Fig. 2e. The spots corresponding to the {111} planes with an interreticular spacing of 0.318 nm (zone axis [01-1]) confirm the presence of the α-phase. The spots corresponding to other plane families such as {200}, {022}, {222}, {311}, etc. are also observed.

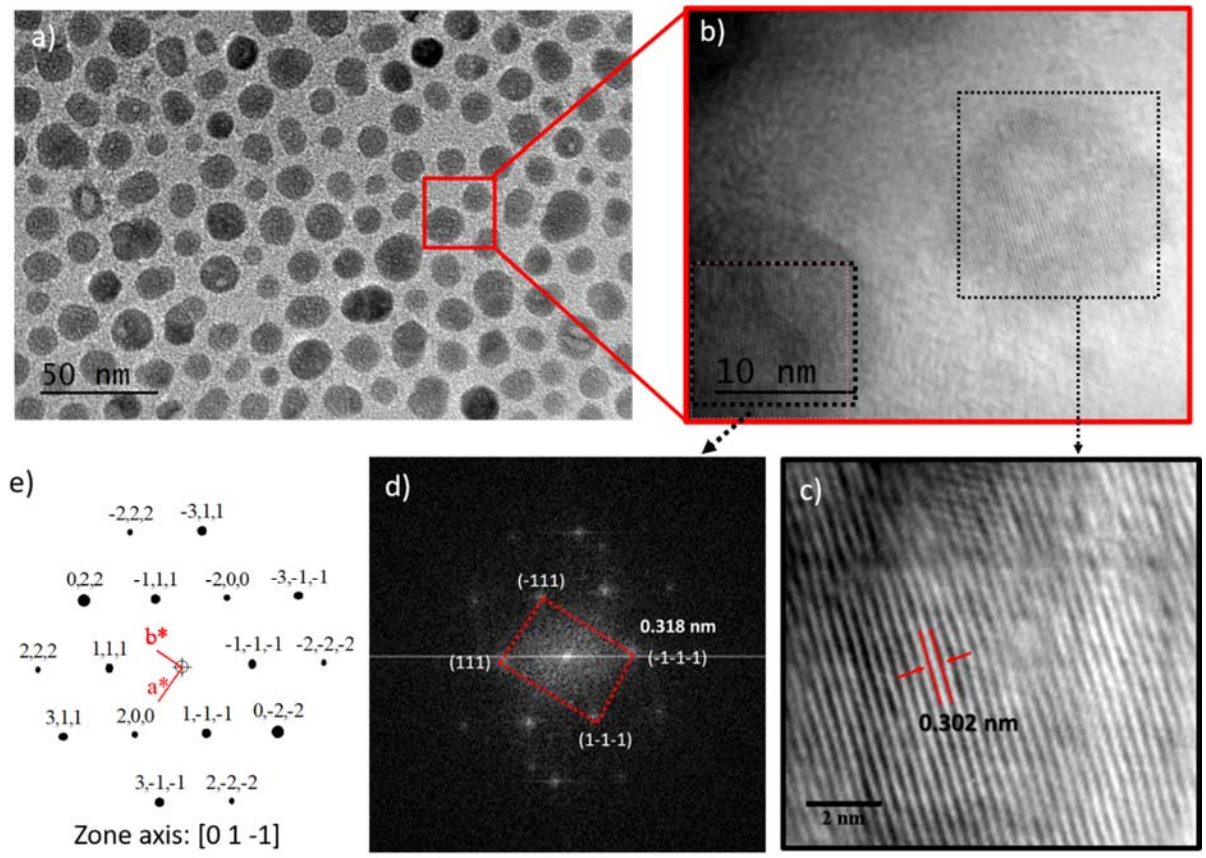

Figure 2. TEM, HR-TEM and associated FFT of the $NaGd_{5/6}Yb_{1/6}F_4$: 0.8%Tm^{3+} NPs obtained from the thermal decomposition of the single source precursors (SSP) [$NaLn(TFA)_4$(diglyme)] (Ln = Gd, Yb, Tm) at 290°C in a 1:1 mixture of 1-octadecene + oleylamine. The HR-TEM image in (c) shows an inter-reticular spacing of 0.302 nm related to the β-phase, whereas the FFT of the second particle in (d) corresponds to the diffraction pattern of a cubic crystal structure (α-phase) in the zone axis [01-1] (e).

3.2. Hydrous synthesis of $NaGdF_4$: Yb^{+3}, Tm^{+3} NPs from the co-precipitation reaction of hydrated inorganic salts at room temperature: To understand the relationship between the synthetic conditions and the structure and morphology of the nanoparticles and their influence over up-conversion efficiency, we have also synthesized the $NaGdF_4$: Yb^{+3}, Tm^{+3} NPs from a modified

co-precipitation method by reacting $Ln(NO_3)_3 \cdot 5H_2O$ (Ln = Gd, Tm, Yb), $NaNO_3$ and NH_4F at room temperature in ethylene glycol [30]. In the powder XRD of the as-prepared powder, abbreviated as UC_hyd NPs, all peaks could be indexed with the β-phase of $NaGdF_4$ (ICDD # 00-027-0699, Fig. 3). Usually, nanostructures synthesized at low temperature are more likely to contain a higher amount of surface defects [31]. Since the synthesis was carried out at room temperature, the crystallinity of the as-obtained powders was slightly lower than that of the UC_anhyd NPs which were obtained by decomposition at elevated temperature. In contrast to the thermal decomposition method, the different dopant percentages had no effect on the crystalline phase of the the UC_hyd NPs in the coprecipitation method (Fig. 3). The TEM images show a very different shape, size and morphology of the UC_hyd NPs (agglomerated nanorods with average size of 197 ± 29 nm in length and 85 ± 10 nm in width versus uniform spherical anhydrous NPs of less than 15 nm, Fig. 4, S5, S6). This agglomeration and formation of large particle size can be attributed to the absence of any effective capping ligand during the room temperature synthesis. Although the presence of ethylene glycol ligand on the surface of the NPs has been confirmed by IR spectra and TG-DTA studies (Fig. S7 and S8), it is less efficient in controlling the nanoparticle size than the capping ligands such as oleic acid (OA) or oleylamine (OM) used in the thermal decomposition method. In Fig. 4d, the FFT pattern of a representative sample i.e., $NaGd_{5/6}Yb_{1/6}F_4$: 0.8% Tm^{3+} shows the diffraction pattern of a hexagonal crystal structure (β-phase) in the zone axis [001]. The spots correspond to {110} plane family with an interreticular distance of 0.29 nm and confirm the β-phase.

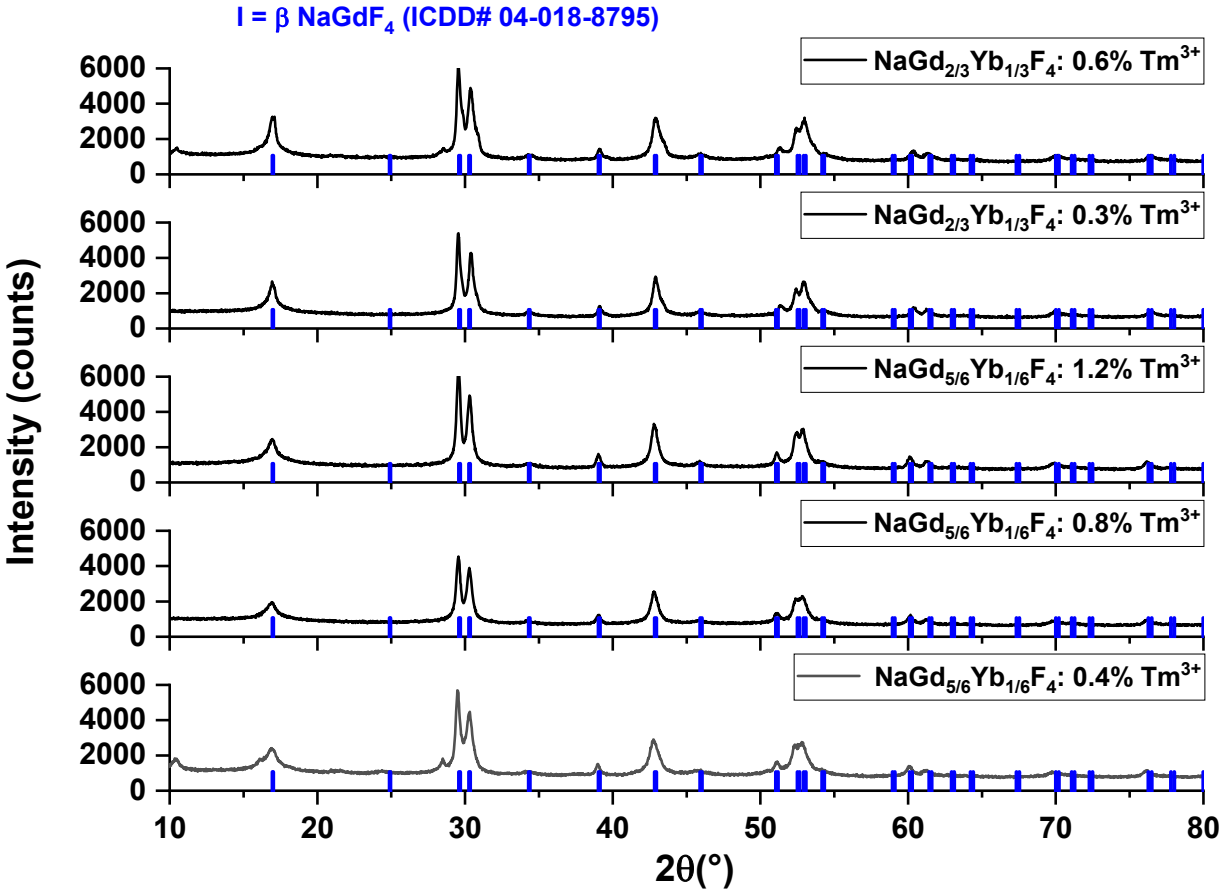

Figure 3. Powder XRD of $NaGdF_4$: Yb^{3+}, Tm^{3+} NPs obtained from co-precipitation reaction of hydrated inorganic salts at room temperature.

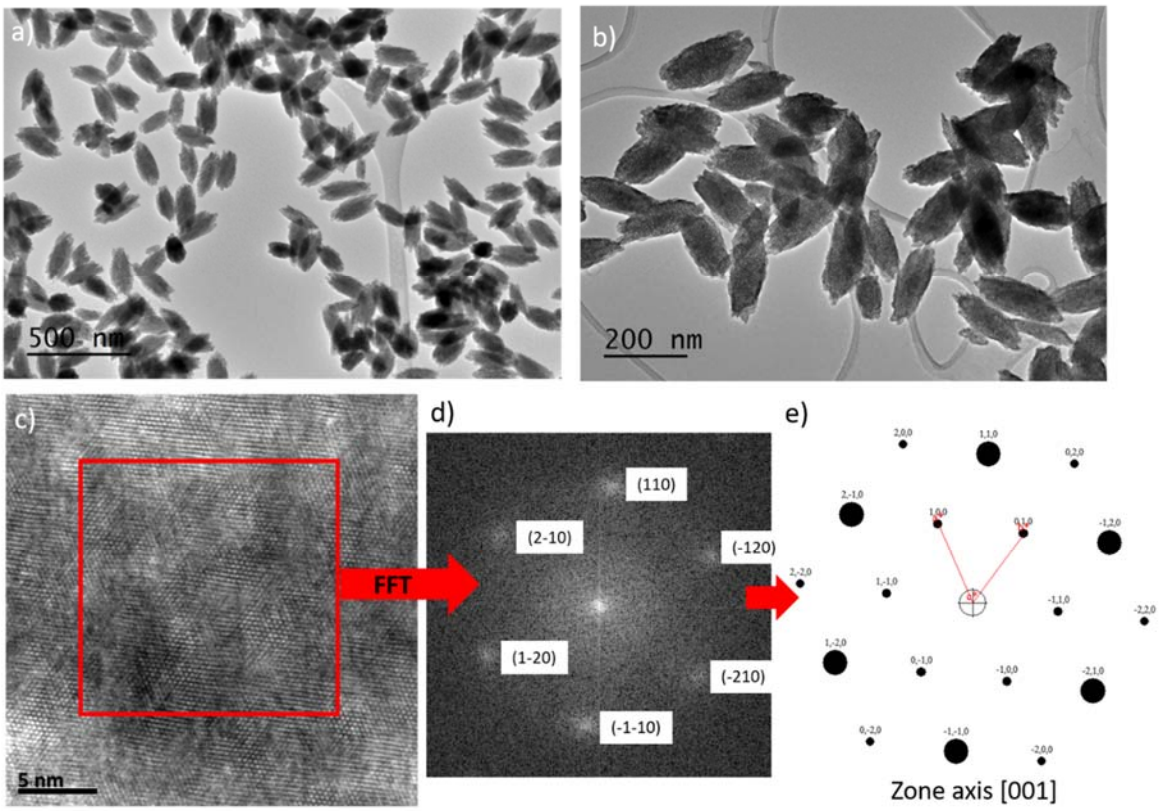

Figure 4. TEM images of $NaGd_{5/6}Yb_{1/6}F_4$: 1.2% Tm^{3+} (a) and $NaGd_{5/6}Yb_{1/6}F_4$: 0.8% Tm^{3+} (b) NPs obtained from room temperature co-precipitation using hydrated inorganic salts $Ln(NO_3)_3 \cdot 5H_2O$ (Ln = Gd, Tm, Yb), $NaNO_3$ and NH_4F in ethylene glycol. HR-TEM (c) and associated FFT analysis (d) of β-$NaGd_{5/6}Yb_{1/6}F_4$: 0.8% Tm^{3+} NPs. The FFT corresponds to the diffraction pattern of a hexagonal crystal structure (β-phase) in the zone axis [001] (e).

3.3. Comparative up-conversion studies. A detailed and systematic study of up-conversion was performed on UC_anhyd and UC_hyd NPs obtained by thermal decomposition of anhydrous precursors in the mixture of 1-octadecene + oleylamine as well co-precipitation method using hydrated inorganic salts in ethylene glycol, respectively (Fig. 5, S9). We observed varying emission intensity profiles for different concentration of doping lanthanide ions (both sensitizer and activator). As up-conversion emission is highly geometry (phase) dependent [32-35], we tried to

observe a variation in the photoluminescence emission profiles and found a trend in the emission profiles by changing the composition of the nanoparticles one by one. From Fig. 5, it is clear that doubling the doping amount of the sensitizer Yb^{3+} quenches the overall up-conversion, probably because of energy transfer within the sensitizer ions themselves. At the same time, the increase in the concentration of activator Tm^{3+} ions from 0.4% to 1.2% (in both $NaGd_{5/6}Yb_{1/6}F_4$ and $NaGd_{2/3}Yb_{1/3}F_4$ series) plays a role in the final up-conversion emission profile. It is, therefore, crucial to obtain an optimal ratio of dopant ions to achieve the highest upconversion efficiency [36]. A careful analysis of Fig. 5 reveals that ~17% Yb^{3+} and 0.8% Tm^{3+} is the optimal ratio of sensitizer and activator to obtain the best up-conversion efficiency in the UC_anhyd NPs studied here. Therefore, this ratio was chosen to compare up-conversion emission for anhydrous and hydrous samples. It should be noted that spectra of all the anhydrous samples given in the Fig. 5 were measured under similar conditions, and hence are comparable. The same is true for spectra of the hydrous samples given in the Fig. S9. However, the spectra given in the Fig. 5 and S9 should not be compared with each other without taking into account the experimental details, notably the slit width.

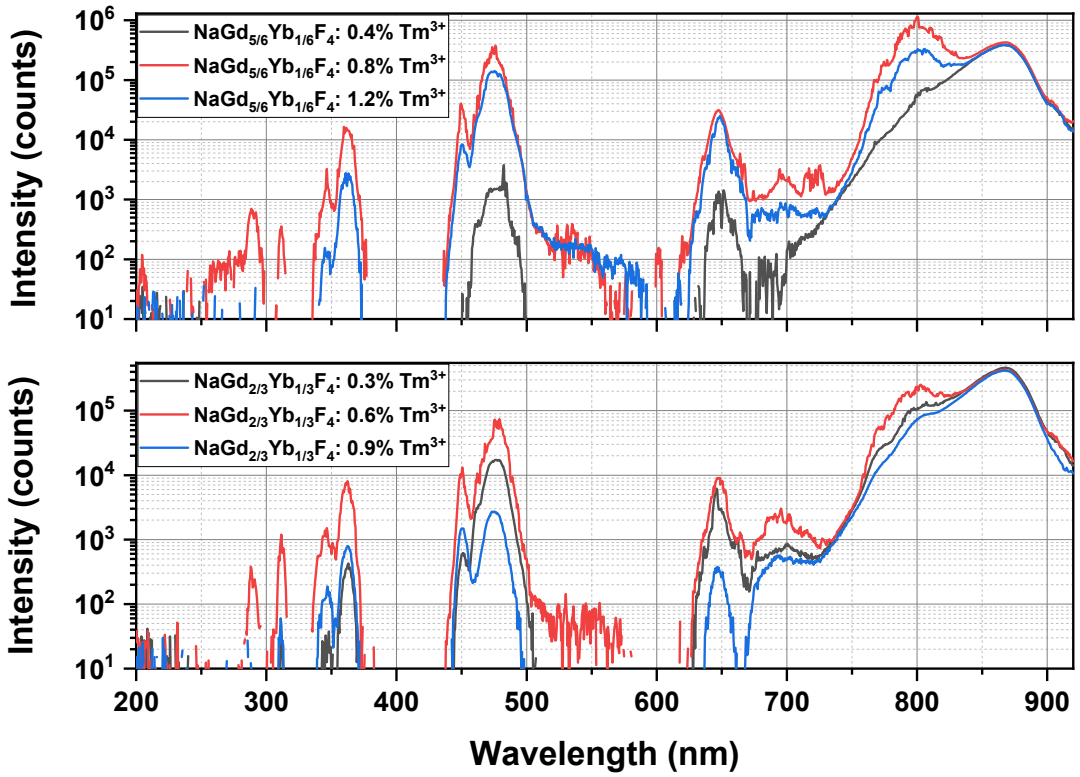

Figure 5. Up-conversion studies (λ_{exc} = 972 nm CW Laser, and slit width = 0.5 mm for entry and exit) of $NaGdF_4$: Yb^{3+}, Tm^{3+} NPs obtained from the thermal decomposition method.

Up-conversion emission spectra of $NaGd_{5/6}Yb_{1/6}F_4$: 0.8% Tm^{3+} NPs synthesized under anhydrous and hydrous conditions were measured in the solid state under 972 nm CW laser excitation (power density = 16.5 W/cm^2). Usually, at high laser intensities, the up-conversion response of the material changes. The local photothermal heating causes modulation in the crystal structure, and hence changes the up-conversion emission response [37]. In our study also, we observed that the hydrous samples started decomposing at moderately higher intensities (>20W/cm^2) while the anhydrous nanoparticles were quite stable even at high laser intensities. The less stability of the hydrous samples may be attributed to their significantly low quantum yield, which would convert most of the energy to heat and, therefore, overheat the samples and

decompose them. The peaks in the spectra of Fig. 6 can be ascribed to the different transitions that occur in the 4f energy levels of the lanthanide ions in the $NaGdF_4$ matrix [24]. It can be seen that these two samples, $NaGd_{5/6}Yb_{1/6}F_4$: 0.8% Tm^{3+}_anhyd and $NaGd_{5/6}Yb_{1/6}F_4$: 0.8% Tm^{3+}_hyd, exhibit emission peaks of significantly different intensity but at exactly similar positions centered around 362 nm in the UV region which is governed by the $^1D_2 \rightarrow {}^3H_6$ transition, around 475 nm corresponding to the $^1G_4 \rightarrow {}^3H_6$ transition and at longer wavelength such as around 650, 698 and 802 nm, representing the $^1G_4 \rightarrow {}^3F_4$, $^1D_2 \rightarrow {}^3H_4$ (or $^3F_3 \rightarrow {}^3H_6$) and $^3H_4 \rightarrow {}^3H_6$ transitions, respectively, from the Tm^{3+} ions. Apart from these strong emission peaks, a few peaks were observed in the deep UV region. The peaks at 290 nm and 348 nm are due to electronic transitions in the Tm^{3+} ions from $^1I_6$ to $^3H_6$ and $^3F_4$, respectively. These peaks were absent in the $NaGd_{5/6}Yb_{1/6}F_4$: 0.8% Tm^{3+}_hyd sample. In addition, a very sharp emission at 312 nm corresponding to $^6P_{7/2} \rightarrow {}^8S_{7/2}$ of the Gd^{3+} ions is present only in the $NaGd_{5/6}Yb_{1/6}F_4$: 0.8% Tm^{3+}_anhyd sample. As shown in the Fig. 6, the up-conversion emission for the $NaGd_{5/6}Yb_{1/6}F_4$: 0.8% Tm^{3+}_anhyd sample, even with its unfavorable characteristics such as mixed α- and β-phase of the matrix and smaller particle size, is much higher than that of the $NaGd_{5/6}Yb_{1/6}F_4$: 0.8% Tm^{3+}_hyd sample. It is well-known that the UC emission intensity of β-$NaLnF_4$ is about an order of magnitude stronger as compared to the α-$NaLnF_4$ host lattice due to longer Ln–F distances and a higher coordination number [38] and the smaller particles usually have lesser up-conversion efficiency owing do their high surface/volume ratio [19]. Compared to the UC_anhyd spherical nanoparticles, the significant reduction in the emission intensity for UC_hyd nanorods can be attributed to a) irregular surface that results in the generation of defect energy levels next to the Tm^{3+} energy levels [33-35], and b) the presence of significant amount of OH^- ions on the surface, as confirmed by the FT-IR and TG-DTG curves (Fig. S7 and S8), competing with the emission of

sensitizer Yb^{3+} ions [39,40].

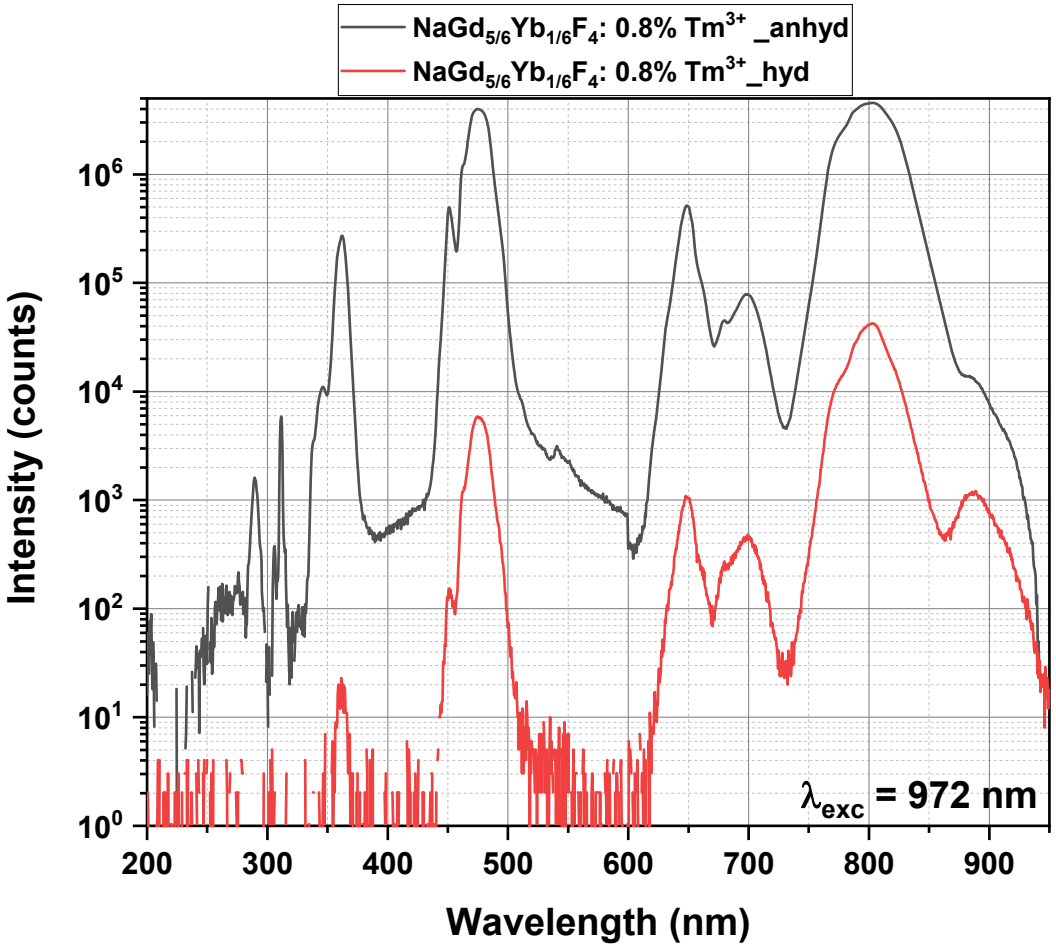

Figure 6. Up-conversion studies comparing the emission intensity of $NaGd_{5/6}Yb_{1/6}F_4$: 0.8% Tm^{3+}_anhyd and $NaGd_{5/6}Yb_{1/6}F_4$: 0.8% Tm^{3+}_hyd samples (slit width = 1 mm for both entry and exit).

Following the qualitative evaluation of the up-conversion emission measurement, we also attempted to quantitatively measure the quantum yield of $NaGd_{5/6}Yb_{1/6}F_4$: 0.8% Tm^{3+}_anhyd and $NaGd_{5/6}Yb_{1/6}F_4$: 0.8% Tm^{3+}_hyd samples with different excitation power densities under otherwise identical conditions to obtain optimal performance. The up-conversion quantum yield was measured using the method originally described by Boyer *et al* [41] and modified accordingly

by Purohit *et al* [42]. Measurements were made at three different intensities for each sample, which are summarized in Table 2 and Table 3. While the term quantum yield (Φ_λ) refers to the ratio of number of photons emitted to the total number of photons absorbed (eq. 1), the energy conversion efficiency (ECE) at a particular wavelength is the measure of how much of the input energy (absorbed by the sensitizers) is converted to the output energy (emitted by the activators) (eq. 2) [43].

$$\Phi_\lambda = \frac{\text{number of photon emitted}}{\text{number of photon absorbed}} \qquad (1)$$

Where λ is the wavelength of the photons at which the quantum yield is measured.

$$\eta_\lambda\,(\mathrm{ECE}_\lambda) = \frac{\text{output energy}}{\text{input energy}} \qquad (2)$$

The power dependent up-conversion quantum yield (Φtotal) values for the $NaGd_{5/6}Yb_{1/6}F_4$: 0.8% Tm^{3+}_anhyd sample, which range from 0.6% to 1.8% for the power density varying from 4.2W/cm^2 to 26.9W/cm^2, are superior to those of $NaGd_{5/6}Yb_{1/6}F_4$: 0.8% Tm^{3+}_hyd sample by a factor of 100 (NIR-to-visible light conversion) or more (NIR-to-UV conversion). As noted before, this can mainly be attributed to the presence of significantly less amount of hydroxyl groups on the surface of the former sample. These up-converting NPs respond differently at higher power densities, particularly the hydrous ones, which show a considerable quenching of the up-conversion emission due to local heating of the sample [37]. Usually, the small size of nanoparticles has very low quantum yield compared to their bulk counterpart [44]. So ideally, surface passivation via core shell formation [45] or use of bulk counterparts is the key strategy to

enhance the quantum efficiency, although it might limit their applications. This approach of synthesizing UC materials using anhydrous precursors thus enables the use of even smaller up-converting NPs for many applications like photocatalysis [24] where their use previously was highly limited.

Table 2. Up-conversion Quantum yield (QY) and energy conversion efficiency (ECE) of $NaGd_{5/6}Yb_{1/6}F_4$: 0.8% Tm^{3+}_anhyd at different power densities of the IR laser for different spectral regions: the under-script UV represents the region between 250 and 375 nm, 475 corresponds to the region 430-530 nm, 648 to the region 635-665 nm, 700 to the region 670-720 nm, 802 to the region 730-870 nm. Finally total stands for the whole 250-900 nm region.

Intensity (W/cm^2)	**Φ_{total} ECE_{total}**	**Φ_{UV} ECE_{UV}**	**Φ_{475} ECE_{475}**	**Φ_{648} ECE_{648}**	**Φ_{700} ECE_{700}**	**Φ_{802} ECE_{802}**
26.9	0.018(3)	$1.3(2) \times 10^{-5}$	$3.4(7) \times 10^{-4}$	$1.1(2) \times 10^{-4}$	$1.5(3) \times 10^{-4}$	0.017(3)
	0.023(4)	$3.5(7) \times 10^{-5}$	$7(14) \times 10^{-4}$	$1.7(3) \times 10^{-4}$	$2.1(4) \times 10^{-4}$	0.021(4)
10.3	0.011(2)	$2.7(5) \times 10^{-6}$	$2.2(4) \times 10^{-4}$	$5.9(12) \times 10^{-5}$	$2.5(5) \times 10^{-5}$	0.010(2)
	0.013(2)	$7.3(14) \times 10^{-6}$	$4.6(9) \times 10^{-4}$	$8.9(18) \times 10^{-5}$	$3.6(7) \times 10^{-5}$	0.013(2)
4.2	0.005(1)	$2.9(6) \times 10^{-7}$	$5.4(10) \times 10^{-5}$	$1.6(3) \times 10^{-5}$	$8.2(16) \times 10^{-6}$	0.005(1)
	0.006(1)	$8.1(16) \times 10^{-7}$	$1.1(2) \times 10^{-4}$	$2.4(5) \times 10^{-5}$	$1.1(2) \times 10^{-5}$	0.006(1)

Table 3. Up-conversion Quantum yield (QY) and energy conversion efficiency (ECE) of $NaGd_{5/6}Yb_{1/6}F_4$: 0.8% Tm^{3+}_hyd at different power densities of the IR laser for different spectral regions: the under-script UV represents the region between 250 and 375 nm, 475 corresponds to the region 430-530 nm, 648 to the region 635-665 nm, 700 to the region 670-720 nm, 802 to the region 730-870 nm. Finally, total stands for the whole 250-900 nm region.

Intensity (W/cm^2)	**Φ_{total} ECE_{total}**	**Φ_{UV} ECE_{UV}**	**Φ_{475} ECE_{475}**	**Φ_{648} ECE_{648}**	**Φ_{700} ECE_{700}**	**Φ_{802} ECE_{802}**

29.4	0.0004(1)	9.0(18) x 10^{-9}	4.1(8) x 10^{-7}	6.4(12) x 10^{-7}	1.8(4) x 10^{-5}	0.00034 (7)
	0.00049(10)	2.4(5) x 10^{-8}	8.5(17) x 10^{-7}	9.5(20) x 10^{-7}	2.5(5) x 10^{-5}	0.00040 (8)
10.9	0.00073(15)	4.2(8) x 10^{-9}	7.0(14) x 10^{-7}	5.2(10) x 10^{-7}	6.2(12) x 10^{-6}	0.00070 (14)
	0.00089(18)	1.1(2) x 10^{-8}	1.4(3) x 10^{-6}	7.8(16) x 10^{-7}	8.7(17) x 10^{-6}	0.00085 (17)
4.2	0.00085(17)	2.4(5) x 10^{-9}	7.4(15) x 10^{-7}	4.6(9) x 10^{-7}	2.0(4) x 10^{-6}	0.00083 (17)
	0.00103(2)	7.1(14) x 10^{-9}	1.5(3) x 10^{-6}	6.9(14) x 10^{-7}	2.9(6) x 10^{-6}	0.0010 (2)

4. Conclusions

In this comparative study, we report the synthesis of up-converting $NaGdF_4$ nanoparticles containing variable ratios of Yb^{+3} and Tm^{+3} ions by two different methods (thermal decomposition of anhydrous single source precursors and co-precipitation at room temperature using hydrated inorganic salts) and the influence of synthetic conditions on the structure and morphology of the nanoparticles as well as the up-conversion efficiency. Bottom-up synthesis using anhydrous molecular precursors in appropriate ratio and solvent(s) not only allows better control of the composition, structure and morphology of $NaGdF_4$: Yb^{+3}, Tm^{+3} nanoparticles, including selective access to pure α-, pure β- or mixed α + β crystalline phases with defined ratios, but the anhydrous conditions also reduce –OH functionality on the surface to significantly enhance their up-conversion efficiency. This study validates the anhydrous precursor approach as a strategy to obtain small but highly emitting up-converting particles without requiring a silica or undoped matrix surface passivation layer, which would be beneficial for the applications that require the

construction of additional layers of another material, e.g., TiO_2@UC NPs type core-shell structure for IR-induced photocatalysis.

Acknowledgements

The authors thank Y. Aizac and F. Bosselet of IRCELYON for powder XRD data.

Funding

This work was supported by the Agence Nationale de la Recherche through the grant number ANR-17-CE09-0002.

Declaration of Competing Interest

There are no interests to declare.

Data availability

The raw/processed data required to reproduce these findings cannot be shared at this time as the data also forms part of an ongoing study.

References

[1] Z. Li, T. Liang, Q. Wang, Z. Liu, Strategies for constructing upconversion luminescence nanoprobes to improve signal contrast, Small 16 (2020) 1905084.

[2] K. Zhenga, K.Y. Loh, Y. Wang, Q. Chen, J. Fan, T. Jung, S.H. Nam, Y.D. Suh, X. Liu, Recent advances in upconversion nanocrystals: Expanding the kaleidoscopic toolbox for emerging applications, Nano Today 29 (2019) 100797.

[3] X. Zhu, J. Zhang, J. Liu, Y. Zhang, Recent progress of rare-earth doped upconversion nanoparticles: Synthesis, optimization, and applications, Adv. Sci. 6 (2019) 1901358.

[4] E. Andresen, U. Resch-Genger, M. Schaferling, Surface modifications for photon-upconversion-based energy-transfer nanoprobes, Langmuir 35 (2019) 5093−5113.

[5] Q. Zhang, F. Yang, Z. Xu, M. Chaker, D. Ma, Are lanthanide-doped upconversion materials good candidates for photocatalysis? Nanoscale Horiz. 4 (2019) 579-591.

[6] Z. Zhang, S. Shikha, J. Liu, J. Zhang**,** Q. Mei**,** Y. Zhang**,** Upconversion nanoprobes: Recent advances in sensing applications, Anal. Chem. 91 (2019) 548-568.

[7] Y. Wang, K. Zheng, S. Song, D. Fan, H. Zhang, X. Liu, Remote manipulation of upconversion luminescence, Chem. Soc. Rev. 47 (2018) 6473—6485.

[8] S. Wen, J. Zhou, K. Zheng, A. Bednarkiewicz, X. Liu, D. Jin, Advances in highly doped upconversion nanoparticles, Nature Commun. 9 (2018) 2415.

[9] N.M. Idris, M.K.G. Jayakumar, A. Bansal, Y. Zhang, Upconversion nanoparticles as versatile light nanotransducers for photoactivation applications, Chem. Soc. Rev. 44 (2015) 1449-1478.

[10] X. Li, F. Zhang, D. Zhao, Lab on upconversion nanoparticles: Optical properties and applications engineering via designed nanostructure, Chem. Soc. Rev. 44 (2015) 1346-1378.

[11] D. Yang, P. Ma, Z. Hou, Z. Cheng, C. Li, J. Lin, Current advances in lanthanide ion (Ln^{3+})-based upconversion nanomaterials for drug delivery, Chem. Soc. Rev. 44 (2015) 1416-1448.

[12] J. Zhou, Q. Liu, W. Feng, Y. Sun, F. Li, Upconversion luminescent materials: advances and applications, Chem. Rev. 115 (2015) 395-465.

[13] J. Zhou, Z. Liu, F. Li, Upconversion nanophosphors for small-animal imaging, Chem. Soc. Rev. 41 (2012) 1323-1349.

[14] J. Zhou, X.J. Zhu, M. Chen, Y. Sun, F.Y. Li, Water-stable $NaLuF_4$-based upconversion

nanophosphors with long-term validity for multimodal lymphatic imaging, Biomaterials 33 (2012) 6201-6210.

[15] G. Tessitore, G.A. Mandl, M.G. Brik, W. Park, J.A. Capobianco, Recent insights into upconverting nanoparticles: spectroscopy, modeling, and routes to improved luminescence, Nanoscale 11 (2019) 12015–12029.

[16] G. Ledoux, M.F. Joubert, S. Mishra, Upconversion phenomena in nanofluorides, in: A. Tressaud, K.R. Poeppelmeir (Eds.), Photonic and Electronic Properties of Fluoride Materials, Elsevier, 2016, pp. 35-63.

[17] a) Li, Z.; Zhang, Y. An efficient and user-friendly method for the synthesis of hexagonal-phase $NaYF_4$:Yb, Er/Tm nanocrystals with controllable shape and upconversion fluorescence. Nanotechnology 19 (2008) 345606; b) F. Shi, J. Wang, D. Zhang, G. Qin, W. Qin, Greatly enhanced size-tunable ultraviolet upconversion luminescence of monodisperse β-$NaYF_4$:Yb,Tm nanocrystals. J. Mater. Chem. 21 (2011) 13413–13421; c) J. Zhao, Z. Lu, Y. Yin, C. McRae, J.A. Piper, J.M. Dawes, D. Jin, E.M. Goldys, Upconversion luminescence with tunable lifetime in $NaYF_4$:Yb, Er nanocrystals: Role of nanocrystal size. Nanoscale 5 (2013) 944–952.

[18] a) S. Mishra, S. Daniele, Molecular engineering of metal alkoxides for solution phase synthesis of high-tech metal oxide nanomaterials, Chem. Eur. J. (2020), DOI: 10.1002/chem.202000534; b) S. Mishra, S. Daniele, Metal-organic derivatives with fluorinated ligands as precursors for inorganic nanomaterials, Chem. Rev. 115 (2015) 8379-8448; c) S. Gahlot, E. Jeanneau, D. Singh, P.K. Panda, Y.K. Mishra, R. Ahuja, G. Ledoux, S. Mishra, Molecules versus nanoparticles: Identifying a reactive molecular intermediate in the synthesis of ternary coinage metal chalcogenides, Inorg. Chem. 59 (2020) 7727-7738; d) S. Mishra, V. Mendez, E. Jeanneau, V. Caps, S. Daniele, A single source precursor route to group 13 homo- and heterometal oxides as highly

active supports for gold catalyzed aerobic epoxidation of *t*-stilbene, Eur. J. Inorg. Chem. (2013) 500–510: e) S. Mishra, E. Jeanneau, M.H. Berger, J.-F. Hochepied, S. Daniele, Novel heteroleptic heterobimetallic alkoxide complexes as facile single source precursors for Ta^{5+}- doped TiO_2-SnO_2 nanoparticles, Inorg. Chem. 49 (2010) 11184–11189; f) S. Mishra, E. Jeanneau, S. Daniele, V. Mendez, Aminoalkoxo-supported heteroleptic hexanuclear gallium(III) wheel as a synthon for group 13 heterometallics: A rare sol-gel precursor for mixed Al-Ga oxide as a support for gold catalysts, Dalton Trans. 39 (2010) 7440–7443.

[19] I. Halimi, E. M. Rodrigues, S. L. Maurizio, H.-Q. T. Sun, M. Grewal, E.M. Boase, N. Liu, R. Marin, E. Hemmer, Pick your precursor! Tailoring the size and crystal phase of microwave-synthesized sub-10 nm upconverting nanoparticles. J. Mater. Chem. C 7 (2019) 15364–15374.

[20] Z. Wang, A. Meijerink, Concentration quenching in upconversion nanocrystals, J. Phys. Chem. C 122 (2018) 26298−26306.

[21] X. Chen, D. Peng, Q. Ju, F.Wang, Photon upconversion in core–shell nanoparticles, Chem. Soc. Rev. 44 (2015) 1318—1330.

[22] a) F. Vetrone, R. Naccache, V. Mahalingam, C.G. Morgan, J.A. Capobianco, Adv. Funct. Mater. 19 (2009) 2924–2929; (b) X. Li, D. Shen, J. Yang, C. Yao, R. Che, F. Zhang, D. Zhao, Successive layer-by-layer strategy for multi-shell epitaxial growth: Shell thickness and doping position dependence in upconverting optical properties, Chem. Mater. 25 (2013) 106−112; c) C. Cao, Q. Liu, M. Shi, W. Feng, F. Li, Lanthanide-doped nanoparticles with upconversion and downshifting near-infrared luminescence for bioimaging, Inorg. Chem. 58 (2019) 9351-9357.

[23] a) S. Mishra, S. Daniele, G. Ledoux, E. Jeanneau, M.-F. Joubert, Heterometallic Na-Y(Ln) trifluoroacetate diglyme complexes as novel single source precursors for upconverting $NaYF_4$

nanocrystals co-doped with Yb and Er/Tm ions. Chem. Commun. 46 (2010) 3756-3758; b) S. Mishra, G. Ledoux, E. Jeanneau, S. Daniele, M.-F. Joubert, Novel heterometal-organic complexes as first single source precursors for up-converting $NaYF_4$:Yb^{3+}, Er^{3+}/Tm^{3+} nanomaterials. Dalton Trans. 41 (2012) 1490-1502.

[24] Y. Chen, S. Mishra, G. Ledoux, E. Jeanneau, M. Daniel, J. Zhang, S. Daniele, Direct synthesis of hexagonal $NaGdF_4$ nanocrystals from a single-source precursor: Upconverting $NaGdF_4$:Yb^{3+},Tm^{3+} and its composites with TiO_2 for near-IR-driven photocatalysis. Chem. Asian J. 9 (2014) 2415–2421.

[25] a) H. Ayadi, W. Fang, S. Mishra, E. Jeanneau, G. Ledoux, J. Zhang, S. Daniele, Influence of Na^+ ion doping on the phase change and upconversion emissions of the GdF_3: Yb^{3+}, Tm^{3+} nanocrystals obtained from the designed molecular precursors. RSC Adv. 5 (2015) 100535-100545; b) S. Mishra, F. Morfin, V. Mendez, P. N. Swamy, J.-L. Rousset, S. Daniele, Nanometric $NaYF_4$ as an unconventional support for Gold catalysts for oxidation reactions. ACS Omega 4 (2019) 5852-5861.

[26] G. Tessitore, A.-V. Mudring, K.W. Kramer, Upconversion luminescence in sub-10 nm β-$NaGdF_4$:Yb^{3+}, Er^{3+} nanoparticles: an improved synthesis in anhydrous ionic liquids RSC Adv. 9 (2019) 34784–34792.

[27] B. Chen, W. Kong, N. Wang, G. Zhu, F. Wang, Oleylamine-mediated synthesis of small $NaYbF_4$ nanoparticles with tunable size. Chem. Mater. 31 (2019) 4779−4786.

[28] B. Chen, F. Wang, Combating concentration quenching in upconversion nanoparticles, Acc. Chem. Res. 53 (2020) 358−367.

[29] N. Liu, R. Marin, Y. Mazouzi, G.O. Cron, A. Shuhendler, E. Hemmer, Cubic versus hexagonal

– effect of host crystallinity on the T1 shortening behavior of $NaGdF_4$ nanoparticles, Nanoscale 11 (2019) 6794–6801.

[30] P. Du, W. Ran, Y. Hou, L. Luo, W. Li, Eu^{3+}-Activated $NaGdF_4$ nanorods for near-ultraviolet light-triggered indoor illumination. ACS Appl. Nano Mater. 2 (2019) 4275–4285.

[31] W. Niu, S. Wu, S. Zhang, L. Li, Synthesis of colour tunable lanthanide-ion doped $NaYF_4$ upconversion nanoparticles by controlling temperature. Chem. Commun. 46 (2010) 3908–3910.

[32] Y. Sun, Y. Chen, L. Tian, Y. Yu, X. Kong, Q. Zeng, Y. Zhang, H. Zhang, Morphology-dependent upconversion luminescence of ZnO:Er^{3+} nanocrystals. J. Lumin. 128 (2008) 15–21.

[33] F. Wang, J. Wang, X. Liu, Direct evidence of a surface quenching effect on size-dependent luminescence of upconversion nanoparticles. Angew. Chem. Int. Ed. 49 (2010) 7456–7460.

[34] W. Bian, Y. Lin, T. Wang, X. Yu, J. Qiu, M. Zhou, H. Luo, S.F. Yu, X. Xu, Direct identification of surface defects and their influence on the optical characteristics of upconversion nanoparticles. ACS Nano 12 (2018) 3623–3628.

[35] H.-X. Mai, Y.-W. Zhang, L.-D. Sun, C.-H. Yan, Highly efficient multicolor up-conversion emissions and their mechanisms of monodisperse $NaYF_4$:Yb, Er core and core/shell-structured nanocrystals. J. Phys. Chem. C 111 (2007) 13721–13729.

[36] M. Kraft, C. Würth, E. Palo, T. Soukka, U. Resch-Genger, Colour-optimized quantum yields of Yb, Tm Co-doped upconversion nanocrystals, Methods Appl. Fluoresc. 7 (2019) 024001.

[37] Q. Min, J. Lei, X. Guo, T. Wang, Q. Yang, D. Zhou, X. Yu, S.F. Yu, J. Qiu, Q. Zhan, X. Xu, Atomic-level passivation of individual upconversion nanocrystal for single particle microscopic imaging, Adv. Funct. Mater. 30 (2020) 1906137.

[38] A. Aebischer, M. Hostettler, J. Hauser, K.W. Kramer, T. Weber, H.U. Gudel, H.B. Burgi, Structural and spectroscopic characterization of active sites in a family of light-emitting sodium

lanthanide tetrafluorides. Angew. Chem., Int. Ed. 45 (2006) 2802–2806.

[39] S. Wilhelm, M. Kaiser, C. Würth, J. Heiland, C. Carrillo-Carrion, V. Muhr, O.S. Wolfbeis, W.J. Parak, U. Resch-Genger, T. Hirsch, Water dispersible upconverting nanoparticles: Effects of surface modification on their luminescence and colloidal stability. Nanoscale 7 (2015) 1403–1410.

[40] H.-X. Mai, Y.-W. Zhang, R. Si, Z.-G. Yan, L. Sun, L.-P. You, C.-H. Yan, High-quality sodium rare-earth fluoride nanocrystals: Controlled synthesis and optical properties. J. Am. Chem. Soc. 128 (2006) 6426–6436.

[41] J.-C. Boyer, F.C.J.M. van Veggel, Absolute quantum yield measurements of colloidal $NaYF_4$: Er^{3+}, Yb^{3+} upconverting nanoparticles. Nanoscale 2 (2010) 1417-1419.

[42] B. Purohit, Y. Guyot, D. Amans, M.-F. Joubert, B. Mahler, S. Mishra, S. Daniele, C. Dujardin, G. Ledoux, Multicolor solar absorption as a synergetic UV upconversion enhancement mechanism in $LiYF_4$:Yb^{3+}, Tm^{3+} nanocrystals. ACS Photonics 6 (2019) 3126–3131.

[43] K.-L. Wong, J.-C.G. Bünzli, P.A. Tanner, Quantum yield and brightness, J. Lumin. 224 (2020) 117256.

[44] M. Kaiser, C. Würth, M. Kraft, I. Hyppänen, T. Soukka, U. Resch-Genger, Power-dependent upconversion quantum yield of $NaYF_4$:Yb^{3+},Er^{3+} nano- and micrometer-sized particles – measurements and simulations, Nanoscale 9 (2017) 10051–10058.

[45] C. Wurth, S. Fischer, B. Grauel, A.P. Alivisatos, U. Resch-Genger, Quantum yields, surface quenching, and passivation efficiency for ultrasmall core/shell upconverting nanoparticles, J. Am. Chem. Soc. 140 (2018) 4922−4928.

TOC figure

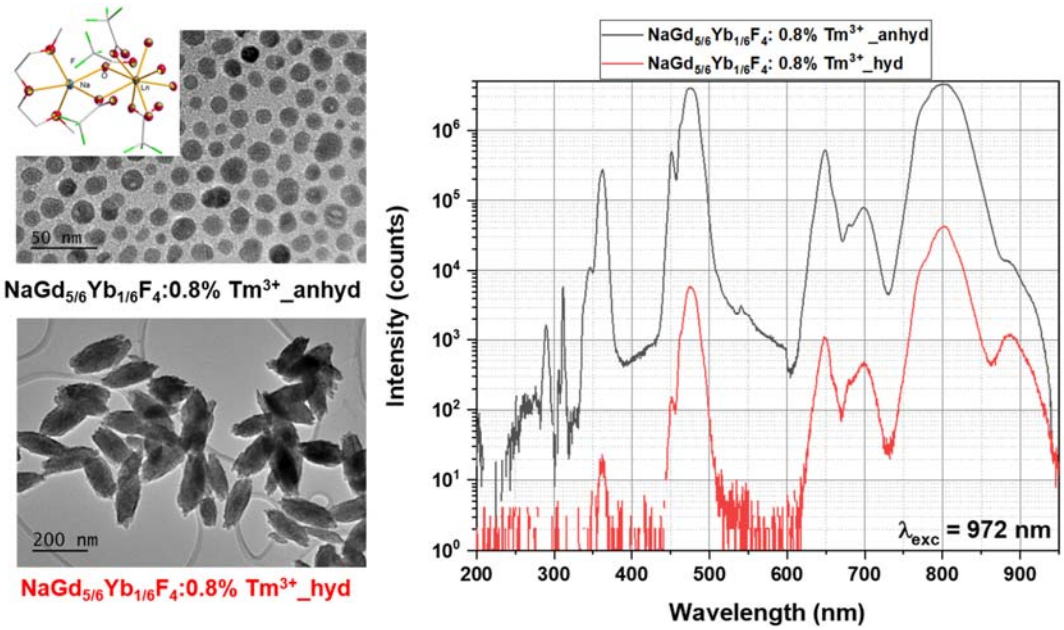
50 nm
NaGd5/6Yb1/6F4:0.8% Tm3+_anhyd
200 nm
NaGd5/6Yb1/6F4:0.8% Tm3+_hyd
NaGd5/6Yb1/6F4: 0.8% Tm3+_anhyd
NaGd5/6Yb1/6F4: 0.8% Tm3+_hyd
Intensity (counts)
Wavelength (nm)
λexc = 972 nm